Chemical Engineering Journal 487 (2024) 150363

Contents lists available at ScienceDirect

Chemical Engineering Journal

journal homepage: www.elsevier.com/locate/cej

Customizing thermometry: Optimizing the operating temperature range of phase transition-based ratiometric luminescence thermometers

L. Marciniak [a,*], W.M. Piotrowski [a], M. Szymczak [a], M. Drozd [a], V. Kinzhybalo [a], M. Back [b]

[a] Institute of Low Temperature and Structure Research, Polish Academy of Sciences, Okolna 2, 50-422 Wroclaw, Poland
[b] Department of Molecular Sciences and Nanosystems, Ca' Foscari University of Venice, via Torino 155, 30172 Venezia-Mestre, Italy

ARTICLE INFO

Keywords:
Luminescence thermometry
Phase transition
Eu3+
First order phase transition

ABSTRACT

Phase transition-based thermometers, which are widely known for their remarkable sensitivity to temperature changes, exhibit a narrow temperature range owing to the stoichiometry of the host material. This limits the applicability of optical sensors utilizing structural phase transitions. In this study, we introduce a co-doping method for modulating the properties of phase transition-based luminescent thermometers to influence the phase transition temperature. We demonstrate that by adjusting the ionic radius of the dopant and its concentration, the transition temperature can be finely tuned across a broad temperature spectrum. The proposed technique enables the customization of luminescent thermometers with enhanced sensitivities and practical temperature ranges tailored to specific user requirements. This study represents a crucial advancement towards the development of personalized luminescence thermometers.

1. Introduction

Luminescence thermometry, a technique that utilizes thermal changes in the luminescent properties of phosphors for temperature measurements, has recently attracted considerable research attention owing to its simplicity, remote readout capability, electrically passive readout, and high reliability [1–8]. Although luminescent thermometry can be potentially used for temperature measurements both in vitro and in vivo as well as in catalytic reactions, combustion chambers of internal combustion engines, microelectronic devices, resistive wire heating, and other applications, ongoing efforts are focused on developing high-sensitivity luminescent thermometers [9–12]. One of the most popular types of luminescence thermometers is a"Boltzmann-type thermometer," in which the intensity ratio of spectral bands used for temperature determination follows a Boltzmann distribution [13–16]. Despite the many advantages of such thermometers, which originate from a fully theoretically predictable calibration curve, their maximum sensitivities are severely limited owing to the constraints of the energy gap between thermally coupled levels [17].

Significantly higher sensitivities were achieved for the thermometers based on two types of luminescent centers [11,18]. However, their sensitivities are insufficient for many applications. Additionally, maximum sensitivities are typically observed within a temperature range corresponding to low-luminescence signals, negatively impacting the thermal resolution. Therefore, a recent study introduced a new solution in luminescence thermometry that utilized changes in the spectroscopic properties of luminescent ions caused by the thermally induced structural phase transitions in the host material [19–22]. The alteration of the local point symmetry of the crystallographic sites occupied by lanthanide (Ln^{3+}) ions used as luminescent dopants during the structural phase transition significantly affects the number of observed Stark lines in individual bands, their splitting strength, and the emission band bandwidth. Studies conducted by Back et al.[19] and Marciniak et al.[20,22] have shown that such structural changes result in highly pronounced changes in the spectroscopic properties of phosphors. Consequently, ratiometric luminescence thermometers based on this approach exhibit very high relative sensitivities. However, because these changes are observed only within the temperature range corresponding to the structural phase transition, the useful temperature range of such thermometers is extremely narrow, limiting their practical applicability. Therefore, it is necessary to devise a new strategy that allows the alteration of the useful temperature range of these thermometers aligning them with specific application requirements. This can be achieved by shifting the phase transition temperature of the host material, which is primarily dependent on its stoichiometry and chemical composition and affects the chemical bond lengths and material

* Corresponding author.
E-mail address: l.marciniak@intibs.pl (L. Marciniak).

https://doi.org/10.1016/j.cej.2024.150363
Received 12 February 2024; Received in revised form 27 February 2024; Accepted 11 March 2024
Available online 12 March 2024

rigidity. Nevertheless, the lack of systematic studies on the regulation of the thermometric properties of phase transition-based ratiometric luminescence thermometers necessitates additional research in this area.

Therefore, we propose a unique strategy for managing the thermometric properties of luminescent thermometers. In our approach, the temperature of the structural phase transition is modulated by co-doping with ions of intentionally different ionic radii as compared with that of the host material cations. Nanocrystalline $LiYO_2$ is considered a model material that undergoes a structural phase transition from monoclinic to tetragonal at approximately 293 K [20–27]. The concept of the proposed approach is schematically illustrated in Fig. 1. The partial substitution of Y^{3+} host cations with ions of smaller (Yb^{3+}) or larger (Gd^{3+}) ionic radii induces a gradual and monotonic shift in the phase transition temperature towards the lower or higher temperatures, respectively. As a result, the intensity ratio of the luminescent bands or luminescence intensity ratio (LIR) of dopant ions (in this case, Eu^{3+}), which serves as the thermometric figure of merit, exhibits pronounced thermal fluctuations within the temperature range corresponding to the phase transition, thus modifying the useful temperature range of the thermometer. Our work demonstrates that the described co-doping method enables the smooth adjustment of the useful temperature range of luminescence thermometers. We believe that the proposed methodology will pave the way for diverse applications of the phase transition-based luminescence thermometers.

2. Experimental

2.1. Synthesis

The powders of $LiYO_2$:1%Eu^{3+}, Yb^{3+} and $LiYO_2$:1%Eu^{3+}, Gd^{3+} nanocrystals were synthesised with a modified Pechini method [28]. Li_2CO_3 (99.9 % purity, Chempur), Y_2O_3 (99.999 % purity, Stanford Materials Corporation), Yb_2O_3 (99.99 % purity, Stanford Materials Corporation), Eu_2O_3 (99.999 % purity, Stanford Materials Corporation), Gd_2O_3 (99.99 % purity, Stanford Materials Corporation), $C_6H_8O_7$ (>99.5 % purity, Alfa Aesar) and $H(OCH_2CH_2)_nOH$, (PEG-200, n = 200, Alfa Aesar) were used as starting materials. Yttrium, ytterbium, gadolinium and europium oxides were dissolved in deionized water with the addition of a small amount of HNO_3 (65 % purity, Avantor), then recrystallized three times to remove the excess of nitrogen. The 4-fold stoichiometric excess of lithium carbonate were added to the water solution of nitrates. After that, an anhydrous citric acid and polyglycol were added to the mixture. The molar ratio of citric acid to all metals was set up as 6:1, meanwhile PEG-200 and citric acid were used in a molar ratio of 1:1. Subsequently, the obtained solution was dried for 3 days at 90 °C until a resin was formed. The produced resin of the samples with Yb^{3+} (1 %; 2 %; 5 %, 10 %; 20 %, 30 %) or Gd^{3+} (1 %; 2 %; 5 %, 10 %; 20 %, 40 %) concentration in respect to the number of Y^{3+} moles ions was annealed in porcelain crucibles for 6 h in air at a temperature of 1000 °C with 10 °C/min heating rate.

2.2. Characterization

Powder diffraction data were obtained in Bragg-Brentano geometry

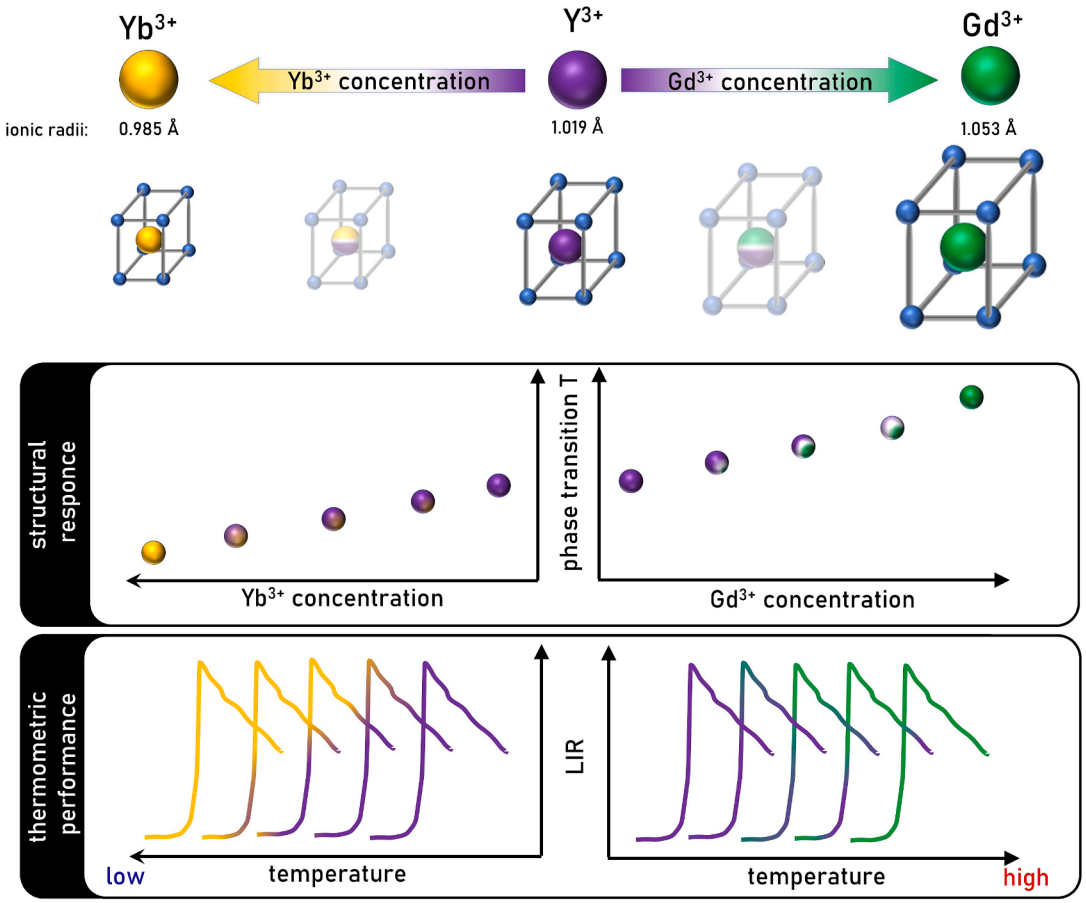

Fig. 1. Conceptual presentation of the strategy to modulate the temperature operating range of the phase transition based ratiometric luminescence thermometer by the host material modification.

using a PANalytical X'Pert Pro diffractometer equipped with Oxford Cryosystems Phenix low-temperature and Anton Paar HTK 1200 N high-temperature attachments using Ni-filtered Cu Kα radiation ($V = 40$ kV, $I = 30$ mA). The sample for low-temperature diffraction experiment was mixed with Apiezon grease. Diffraction patterns in 2θ (15-90°) range were measured in cooling/heating sequence in the temperature range of + 25 to –173 °C. The sample for high-temperature diffraction experiment was measured in 10-90° 2θ range in heating/cooling sequence in the temperature range of + 25 to + 350 °C. ICSD database entries No. 50,992 (LT phase) and 50,993 (HT phase) were taken as initial models for the analysis of the obtained diffraction data. Transmission electron microscope (TEM) images were performed with the Philips CM-20 SuperTwin transmission electron microscope, operating at 160 kV. The sample was ground in a mortar and dispersed in methanol, and then a drop of the suspension was put on a copper microscope grid covered with carbon. Before the measurement, the sample was dried and purified in a H_2/O_2 plasma cleaner for 1 min, 8000 calorimeter equipped with Controlled Liquid Nitrogen Accessory LN2 with a heating/cooling rate of 10 K/min. The measurement was performed for the powder sample in the 100 – 315 K temperature range. A differential scanning calorimetric (DSC) measurements were performed on Perkin-Elmer DSC 8000 calorimeter equipped with Controlled Liquid Nitrogen Accessory LN2 with a heating/cooling rate of 10 K/min. The sample was sealed in the aluminum pans. The measurement was performed for the powder sample in the 80 – 600 K temperature range. The excitation spectra were obtained using the FLS1000 Fluorescence Spectrometer from Edinburgh Instruments equipped with 450 W Xenon lamp and R928 photomultiplier tube from Hamamatsu. Emission spectra were measured using the same system with 395 nm laser diode excitation. To carry out the temperature-dependent measurement, the temperature of the sample was controlled using a THMS600 heating–cooling stage from Linkam (0.1 °C temperature stability and 0.1 °C set point resolution). Luminescence decay profiles were recorded using the FLS1000 Fluorescence Spectrometer from Edinburgh Instruments equipped with 150 W μFlash lamp. The internal quantum yield was measured using the same system supplied with the integrating sphere.

3. Results and discussion

$LiYO_2$ crystallizes into two structures: a low-temperature monoclinic phase (*P21/c* space group) and high-temperature tetragonal phase (*I41/amd* space group (Z = 4)) (Fig. 2a)[23,24,26,27]. In the case of single-

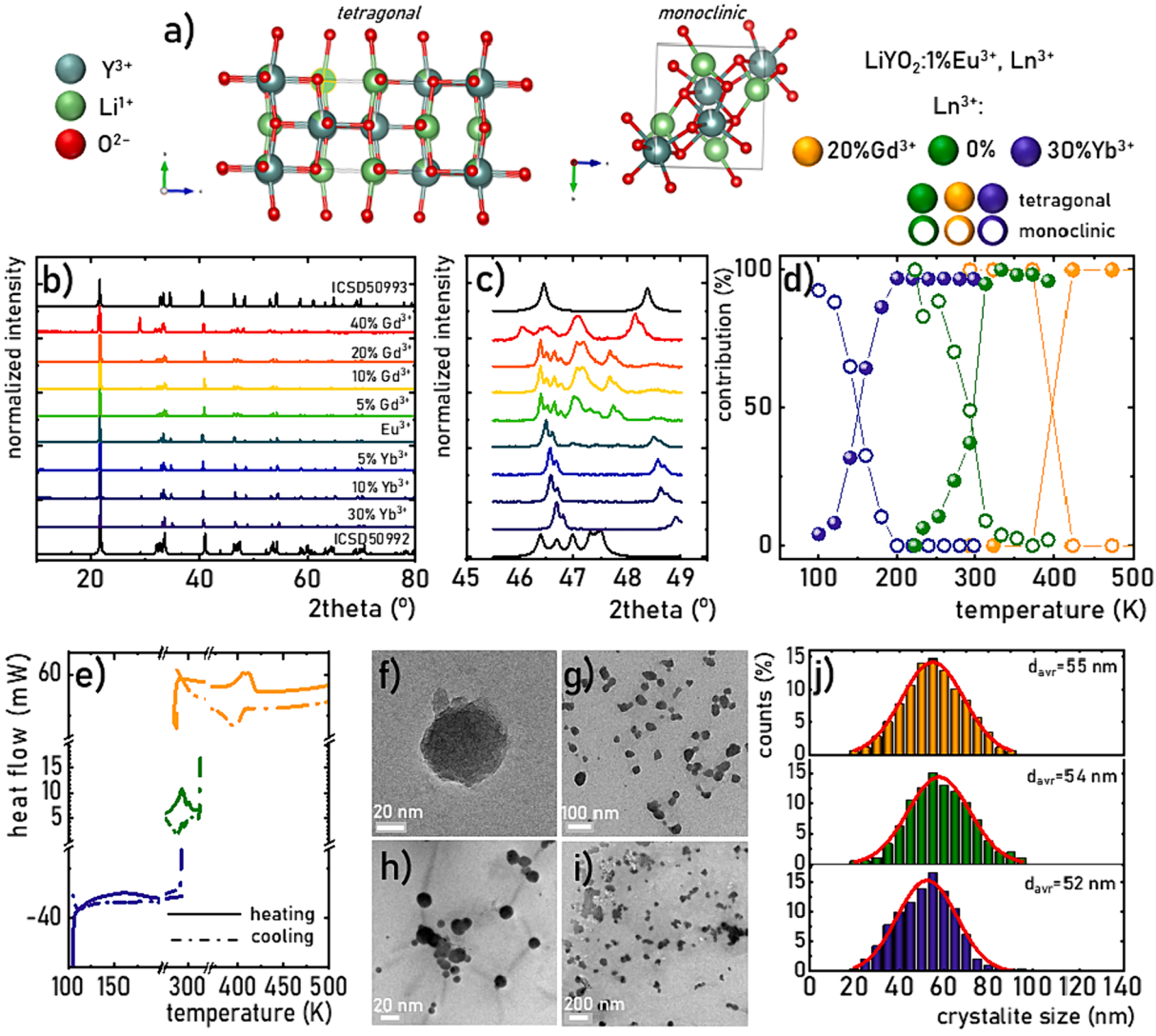

Fig. 2. Visualization of the monoclinic and tetragonal $LiYO_2$ structures-a); the XRD patterns of the $LiYO_2$:1%Eu^{3+}, Ln^{3+} -b) and zoom in the 2theta = 31-36° range -c) thermal dependence of the contribution of monoclinic and tetragonal phases for $LiYO_2$:1%Eu^{3+}, $LiYO_2$:1%Eu^{3+}, 30 %Yb^{3+} and $LiYO_2$:1%Eu^{3+}, 20 %Gd^{3+} -d); DSC data for those samples -e) the representative TEM images for $LiYO_2$:1%Eu^{3+}, 30 %Yb^{3+}-f), g); $LiYO_2$:1%Eu^{3+}, 20 %Gd^{3+}-h), i) and the corresponding particle size distribution -j).

crystal $LiYO_2$, a phase transition occurs at approximately 363 K. However, reducing the size of the luminescent material to nanocrystals with an average crystallite size of approximately 55 nm decreases the phase transition temperature to approximately 293 K. This phase transition induces a reduction in the unit cell parameter *a* and significant elongation along the c-direction (monoclinic a = 6.1493(8) Å, b = 6.1500 (10) Å, c = 6.2494(2) Å, β = 119.091(5)° and tetragonal a = 4.4468(9) Å, c = 10.372(22) Å). Because of this phase transition, the point symmetry of the Y^{3+} cation changes from C_2 to D_{2d} with increasing temperature. This behavior is particularly significant considering the spectroscopic characteristics of lanthanide dopant ions because they preferentially occupy the Y^{3+} positions in the $LiYO_2$ lattice owing to charge matching and the similar ionic radii. This effect is confirmed by the fact that the introduction of high concentrations of Yb^{3+} and Gd^{3+} ions into $LiYO_2$:1%Eu^{3+} does not result in additional reflections in the XRD patterns presented in Fig. 2b (see also Fig. S1-3). However, increasing the concentration of ions with smaller (Yb^{3+}) or larger (Gd^{3+}) ionic radii relative to that of the host Y^{3+} ions decreases or increases the $LiYO_2$ unit cell size manifested as a shift of reflections towards the larger/smaller 2θ values, respectively, in the corresponding XRD patterns (Fig. 2c). Additionally, for the $LiYO_2$:1%Eu^{3+}, Gd^{3+} materials with Gd^{3+} concentrations over 5 %, the room-temperature XRD patterns exhibit reflections associated only with the low-temperature phase. For these materials, the structural phase transition occurs at temperatures higher than room temperature. To verify this hypothesis, temperature-dependent XRD measurements were performed for representative materials, such as $LiYO_2$:1%Eu^{3+}, $LiYO_2$:1%Eu^{3+}, 20 %Gd^{3+}, and $LiYO_2$:1% Eu^{3+}, 30 %Yb^{3+}. Rietveld refinement data indicate that in these structures, a temperature increase gradually increases the contribution of the tetragonal phase relative to the monoclinic phase in the sample volume. However, the host material composition affects the temperature, above which the dominance of the tetragonal phase is observed. As expected, the introduction of Yb^{3+} ions lowers this temperature, whereas Gd^{3+} ions increase it as compared with the value obtained for $LiYO_2$:1%Eu^{3+}. These results indicate a change in the structural phase transition temperature due to the introduction of dopant ions. To support this conclusion, differential scanning calorimetry measurements were performed, unambiguously demonstrating changes in phase transition temperatures between two different samples. For $LiYO_2$:1%Eu^{3+}, 30 % Yb^{3+} the onset of a very weak first-order phase transition was noticed at 153 K during a heating cycle and at 164 K in the cooling process. The enthalpy of this phenomenon is equal to ca 0.3 J/g. In the case of $LiYO_2$:1%Eu^{3+} the heating a peak is observed with onset at 287.5 K. The calculated enthalpies of this peak is equal to 9.43 J/g. During the cooling, the counterparts of observed peaks are noticed at 277.5 K with calculated enthalpy – 7.3046 J/g, respectively. The introduction of Gd^{3+} co-dopant evidently results in an increase of the phase transition temperature. Therefore $LiYO_2$:1%Eu^{3+}, 20 %Gd^{3+} shows that phase transition with non-continuous character is observed at 396 K and 407 K in the heating and cooling cycles, respectively. It should be noted that in this case, the change of enthalpy is equal to ca. 11 J/g.

However, a morphological analysis reveals that increasing the Ln^{3+} dopant concentration does not significantly affect the morphology of the studied materials, indicating that $LiYO_2$:1%Eu^{3+}, Ln^{3+} is composed of nanoparticles with an average grain size of 54 ± 22 nm.

The luminescence characteristics of Eu^{3+} ions result from the *4f–4f* transitions occurring between the $^5D_0$ excited state and ^7F_J multiplets [29]. In the case of the host materials with low phonon energies, additional emission bands related to the radiative depopulation of the $^5D_1$ state are also observed owing to the narrow energy gap between $^5D_0$ and $^5D_1$, which can be non-radiatively bridged in materials with higher phonon energies. In addition to the $^5D_0$ and $^7F_0$ singlet states, the remaining *4f* energy states of Eu^{3+} are split into Stark components in the host material. The number of Stark levels and splitting strength depend on the local ion symmetry. Consequently, for $LiYO_2$:Eu^{3+}, a significantly larger number of Stark components is anticipated in the low-temperature monoclinic phase than in the high-temperature tetragonal phase (Fig. 3a). The increasing quantitative contribution of the high-temperature tetragonal phase of $LiYO_2$:Eu^{3+} observed with increasing temperature causes an increase in the intensity of Stark lines associated with this phase while a simultaneous decrease in the emission intensity of lines associated with the monoclinic phase can be observed until only the signal associated with the tetragonal phase can be noticed. This is particularly well seen in the case of several emission lines, e.g. monoclinic: 536 nm, 563 nm, 591 nm, 621 nm, 559 nm; tetragonal: 566 nm, 587 nm, 621 nm, 662 nm, etc.). This thermally induced structural phase transition in $LiYO_2$:Eu^{3+} is confirmed by the change in the shape of its emission spectrum with temperature (Fig. 3b, Figure S4-11). The spectra are predominantly characterized by the $^5D_0 \rightarrow {}^7F_2$ emission bands at approximately 615 nm. The pronounced intensity of this electric dipole-induced electronic transition with respect to the magnetic dipole-induced electronic transition ($^5D_0 \rightarrow {}^7F_1$ at approximately 590 nm) serves as an indicator of the structural arrangement of Eu^{3+} ions at the non-centrosymmetric crystallographic sites of Y^{3+} ions. The monoclinic-to-tetragonal phase transition signifies an increase in the point symmetry, resulting in a reduction of the $^5D_0 \rightarrow {}^7F_2$ emission band intensity related to the $^5D_0 \rightarrow {}^7F_1$ transition. To better illustrate the spectral changes of Eu^{3+} ions induced by the phase transition in $LiYO_2$, individual bands are depicted in Fig. 3c–f. For the bands associated with the $^5D_1 \rightarrow {}^7F_J$ transitions, a significantly lower number of the observed spectral lines can be distinguished in the tetragonal phase as compared with the monoclinic phase. Nevertheless, owing to their low intensities, these bands are not analyzed in the present study. The $^5D_0 \rightarrow {}^7F_1$ band obtained for the low-temperature phase consists of three distinct Stark components, while in the high-temperature spectra, only two Stark components are observed. A similar reduction in the number of emission lines is detected for the remaining bands; however, the total number of the observed Stark components increases with an increase in the total orbital angular momentum J. For each band, a gradual increase in temperature decreases the intensities of the Stark components associated with the monoclinic structure and increases the intensities of the lines associated with Eu^{3+} ions in the tetragonal structure. However, this transition does not occur across the entire range of the analyzed temperatures but corresponds to the vicinity of the phase transition temperature. This phenomenon is illustrated by the temperature-sensitive luminescence intensity maps presented in Fig. 3g–l, where the spectral range is limited to the $^5D_0 \rightarrow {}^7F_1$ band. The transition temperature is clearly discernible, indicating the appearance of spectral lines associated with the tetragonal structure. However, the phase transition temperature strongly depends on the type and concentration of the Ln^{3+} co-dopant. At a high Yb^{3+} ion concentration (30 %), the transition temperature is approximately 110 K and progressively shifts to 220 K (10 % Yb^{3+}), 250 K (5 % Yb^{3+}), 310 K (1 % Gd^{3+}), and 410 K (20 % Gd^{3+}). For $LiYO_2$:1%Eu^{3+} nanocrystals with 40 % Gd^{3+}, spectral lines originating from the tetragonal phase are not observed across the entire analyzed temperature range (Figure S12-17).

The opposite thermal behavior of the Stark components of Eu^{3+} ions in the monoclinic and tetragonal phases of $LiYO_2$:Eu^{3+} enables the development of ratiometric luminescence thermometers. For the two most intense emission bands, the spectral separation between various Stark components is most favorable for the $^5D_0 \rightarrow {}^7F_1$ emission band owing to the smaller number of its Stark components. In this case, LIR can be defined as a ratiometric figure of merit:

$$LIR = \frac{\int_{587nm}^{589nm} {}^5D_0 \rightarrow {}^7F_1 d\lambda}{\int_{590nm}^{592.5nm} {}^5D_0 \rightarrow {}^7F_1 d\lambda} \quad (1)$$

Regardless of the chemical composition of the host material, LIR exhibits qualitatively similar thermal variations. With increasing temperature, its value abruptly increases, reaching a maximum at the boundary temperature, above which a gradual decrease occurs. Independently of dopant concentration the thermal enhancement of the LIR

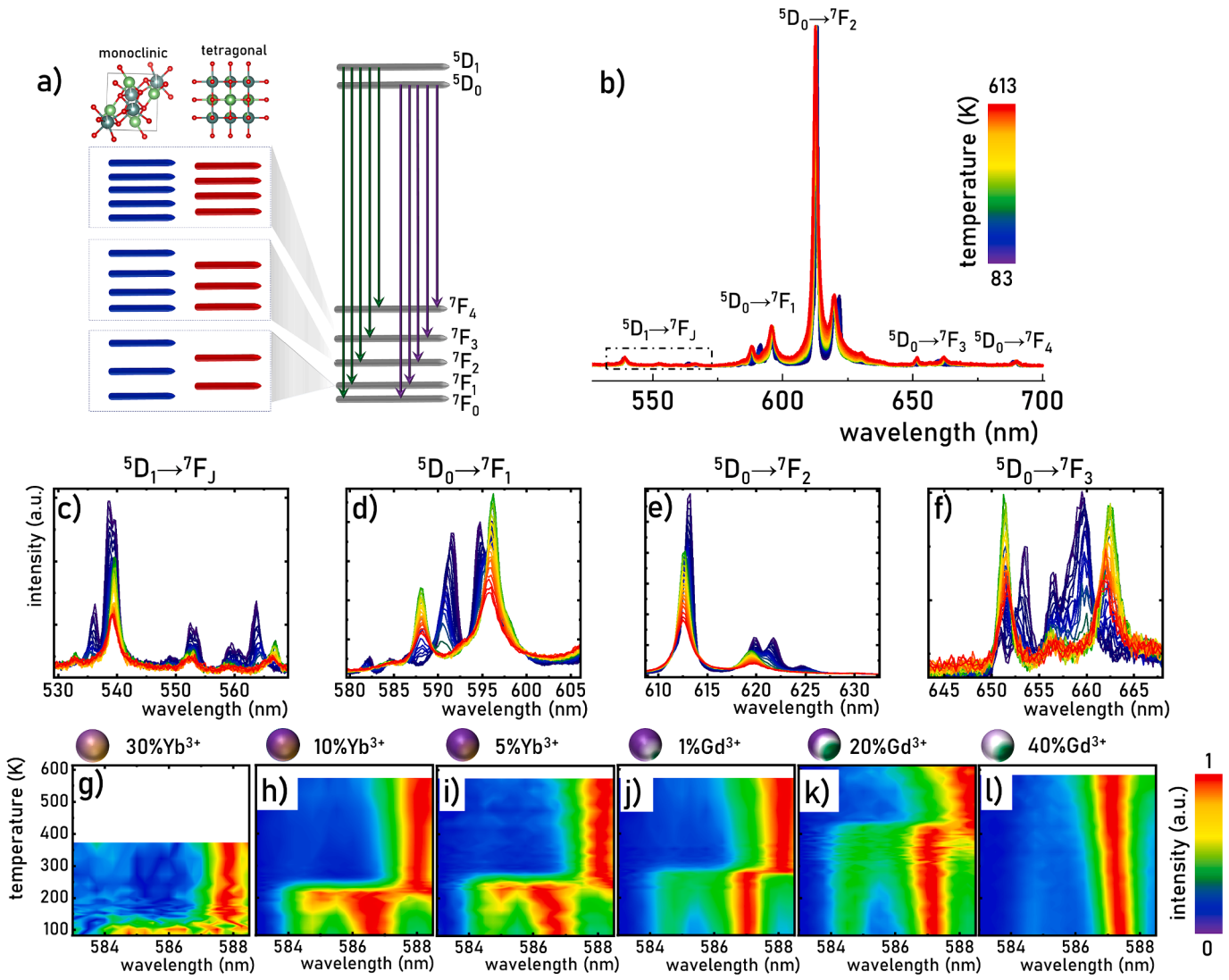

Fig. 3. Simplified energy level diagram of Eu^{3+} ions in monoclinic and tetragonal $LiYO_2$ phases-a), temperature dependent of emission spectra of $LiYO_2$:Eu^{3+} nanocrystals upon λ_{exc} = 395 nm excitation-b) and the spectra limited to the $^5D_0\rightarrow{}^7F_J$-c); $^5D_0\rightarrow{}^7F_1$-d); $^5D_0\rightarrow{}^7F_2$-e); $^5D_0\rightarrow{}^7F_3$-f); the thermal emission intensity maps limited to the 583–588 nm spectral range for $LiYO_2$:1%Eu^{3+}, 30 %Yb^{3+}-g); $LiYO_2$:1%Eu^{3+}, 10 %Yb^{3+}-h); $LiYO_2$:1%Eu^{3+}, 5 %Yb^{3+}-i); $LiYO_2$:1%Eu^{3+}, 1 %Gd^{3+}-j); $LiYO_2$:1%Eu^{3+}, 20 %Gd^{3+}-k); $LiYO_2$:1%Eu^{3+}, 40 %Gd^{3+}-l).

can be described by the allometric function ($LIR(T) = AT^C + B$, where C ~ 24 and A, B, C are fitting parameters). However, the concentration of co-dopant ions affects the LIR thermal variability range, and the maximum LIR enhancement is observed for the $LiYO_2$:1%Eu^{3+} sample. The addition of both Gd^{3+} and Yb^{3+} co-dopant ions reduces the maximum LIR value and the rapidity of the thermal LIR increase (Figure S7 and S14). A comparison of the normalized LIR values clearly indicates that the temperature, at which the maximum LIR value is achieved ($T(LIR_{max})$), shifts monotonically with the co-dopant concentration. The higher concentrations of Yb^{3+} ions reduce lead to the reduction of the $T(LIR_{max})$, whereas the opposite trend is observed with increasing Gd^{3+} ion concentration. This phenomenon is consistent with the structural (Fig. 2) and spectroscopic (Fig. 3) changes resulting from the introduction of co-dopant ions. The monotonic thermal variability of LIR (up to LIR_{max}) obtained for all the analyzed luminophores indicates that LIR can be utilized as a thermometric parameter. Importantly, the useful temperature range of such a thermometer is limited to approximately 100 K and gradually shifts towards the lower/higher temperatures with increasing Yb^{3+}/Gd^{3+} ion concentrations (Fig. 4c). For the analyzed nanocrystals, the useful temperature range can be defined as $T(LIR_{max})$ − 100 K. The obtained results clearly demonstrate that the shift in the phase transition temperature after the introduction of co-dopants with different ionic radii relative to the matrix cation allows the smooth adjustment of the useful temperature range of the ratiometric luminescence thermometer within the range of 80–530 K. Hence, $T(LIR_{max})$ can be successfully controlled over a wide temperature range by adjusting the concentration of lanthanide ions (Ln^{3+}) (Fig. 4d). The monotonic sublinear dependence of $T(LIR_{max})$ on the co-dopant ion concentration clearly indicates that the primary factor regulating $T(LIR_{max})$ is the effective difference between the ionic radii of Ln^{3+} ions and host material cations (Y^{3+}), which is proportional to the concentration of Ln^{3+} ions. This mismatch (Ω) can be expressed using the following equation:

$$\Omega = \frac{R_0 - n\Delta R}{R_0} - 1 \quad (2)$$

where R_0 represents the ionic radius of Y^{3+} ions, and n is the co-dopant ion concentration. The difference between the ionic radii of the host material ions and co-dopant, ΔR, is calculated as follows:

$$\Delta R = R_0 - R_{co-dopant} \quad (3)$$

$T(LIR_{max})$ is a nearly linear function of Ω, confirming that the proposed

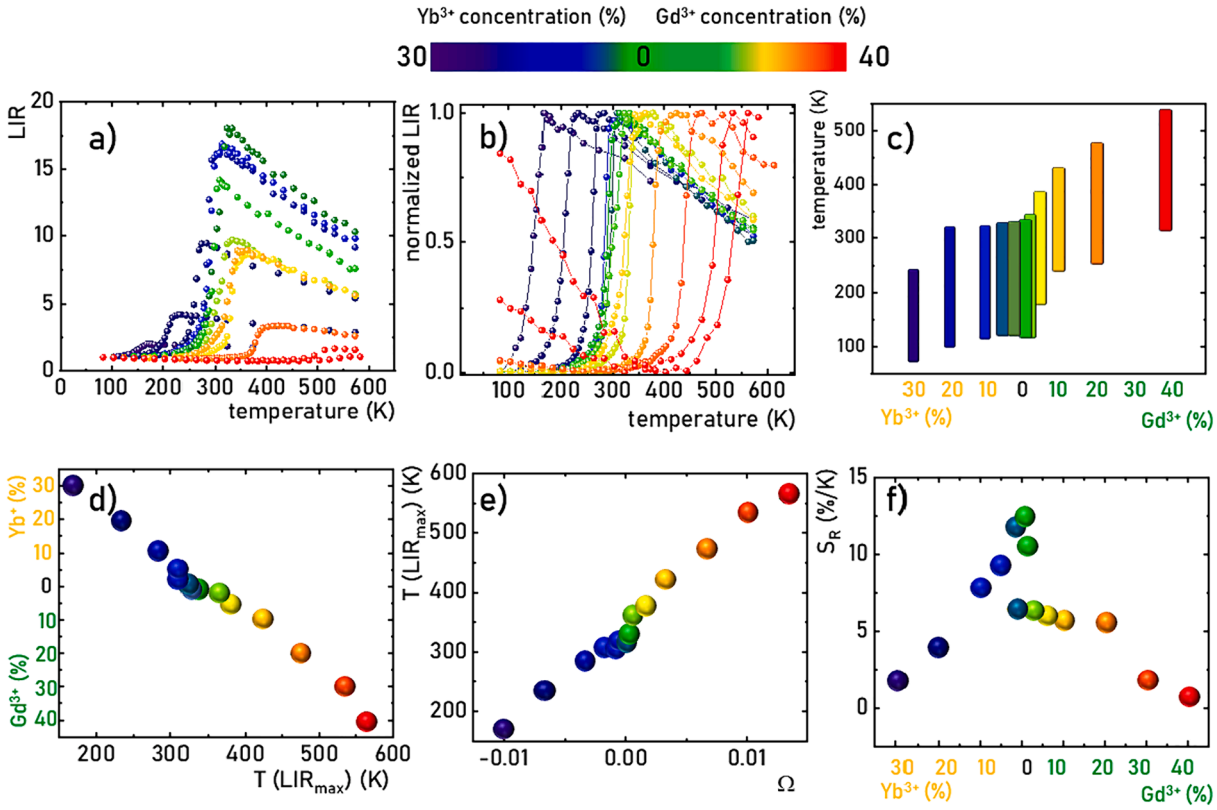

Fig. 4. Absolute -a) and normalized-b) thermal dependence of LIR -a); usable thermal range for LIR based luminescent thermometers-c); temperature of LIR_{max} as a function of co-dopant concentration-d) the $T(LIR_{max})$ as a function of Ω-e; maximal S_R as a function of dopant concentration -f) for different composition of $LiYO_2$:1% Eu^{3+}, Ln^{3+}.

co-doping strategy allows the smooth regulation of the useful temperature range of the ratiometric phase transition-based luminescence thermometer. To quantify the LIR thermal variability and determine the potential applications of the developed luminescence thermometers, the relative sensitivity was determined using the following equation:

$$S_R = \frac{1}{LIR}\frac{\Delta LIR}{\Delta T}\cdot 100\% \quad (4)$$

The maximum relative sensitivity of S_R = 12.5 %/K was obtained for $LiYO_2$:1%Eu^{3+}, which successively decreased with increasing Ln^{3+} ion concentration (the list of the maximal S_R for all samples is presented in Table S1). The maximal value of S_R is observed at temperatures corresponding to the phase transition temperature and except this temperature range much lower sensitivities can be noticed. It can be noticed that the values obtained for low dopant concentration are relatively high comparing to other types of ratiometric luminescence thermometers like those based on the emission of phosphors doped with lanthanide ions [30–32] or transition metal ions [11,33] that do not undergo a structural phase transition. However for Ln^{3+} in $LiYO_2$:1%Eu^{3+}, Ln^{3+} concentration above 20 % the S_R decreases significantly.

Another important factor that enables to evaluate the application potential of a luminescent thermometer for temperature sensing is temperature resolution determined as follows [34]:

$$\delta T = \frac{1}{S_R}\frac{\delta LIR}{LIR} \quad (5)$$

where the δLIR/LIR represents the relative uncertainty of temperature determination and is determined by the uncertainties of the quantification of the individual emission intensities used for LIR determination (I_1 and I_2) as follows:

$$\frac{\delta LIR}{LIR} = \sqrt{\left(\frac{\delta I_1}{I_1}\right)^2 + \left(\frac{\delta I_1}{I_1}\right)^2} \quad (6)$$

The results of the performed calculation shown in Figure S18 reveal that the lowest δT corresponds to the temperature at which the highest S_R was observed. The minimal δT = 0.049 K for $LiYO_2$:1%Eu^{3+} and its value increases with the increase of dopant concentration. However, the highest δT can be found for high doping of Yb^{3+}. This is due to the decrease in the emission intensity of Eu^{3+} ions, which is most likely related to an increase in the probability of Eu^{3+}→Yb^{3+} energy transfer. Due to the lack of energy levels of Gd^{3+} ions occurring below the $^5D_0$ level of Eu^{3+} ions, such an effect is not observed for $LiYO_2$:Eu^{3+},Gd^{3+} samples. This is reflected in the changes in luminescence internal quantum yields for $LiYO_2$:Eu^{3+}, Yb^{3+} and $LiYO_2$:Eu^{3+}, Gd^{3+} samples (Figure S19). In the case of $LiYO_2$:Eu^{3+}, Gd^{3+}, the IQY is about 22 % and does not change significantly with a change in dopant concentration while an increase in the concentration of Yb^{3+} ions results in a decrease in IQY to 5 % for $LiYO_2$:Eu^{3+}, 30 % Yb^{3+}. Therefore, it is advantageous from the perspective of the presented solution to use optically inactive dopant ions.

In addition to the many advantages of the described luminescent thermometers, it is worth mentioning a limitation of the proposed solution. One of the most significant is the fact related to the first-order phase transition mechanism itself, i.e. the hysteresis of the observed transition already manifested in DSC studies (Fig. 1). This effect is also reflected in the LIR hysteresis loop (see Figure S20). This is an important limitation, because if the monotonicity of the LIR variation changes, a situation can occur for which one temperature value corresponds to two LIR values. Therefore, the developed thermometers should be used in applications where the monotonicity of the temperature change is known and does not change during the experiment.

4. Conclusions

In this study, the possibility of modulating the thermometric properties of ratiometric luminescence thermometers based on materials exhibiting thermally induced structural phase transitions was investigated by successively introducing co-dopant ions with ionic radii different from those of the host material cation. The $LiYO_2$:Eu^{3+} system was used as an illustrative example. It was demonstrated that the increase in temperature leading to the transition between the low-temperature monoclinic and high-temperature tetragonal phases was clearly reflected by the changes in the shapes of the luminescence spectra of Eu^{3+} ions. This allowed the development of ratiometric luminescence thermometers with a high sensitivity and relatively narrow useful temperature range (approximately 100 K). However, the introduction of co-dopant ions with the smaller (Yb^{3+}) or larger (Gd^{3+}) ionic radii relative to that of the host material's Y^{3+} ions enabled a proportional shift in the phase transition temperature towards the lower or higher values, respectively. The analysis conducted revealed that the temperature, at which the maximum LIR value was achieved, was sub-linearly proportional to the ionic mismatch between the co-dopant ions Ω. The proposed strategy allows the smooth adjustment of the useful temperature range of luminescence thermometers based on the phase transition in $LiYO_2$:Eu^{3+}, enabling the development of luminescence thermometers with customizable thermometric parameters. The sub-linear correlation between $T(LIR_{max})$ and Ω suggests that this strategy is universal for other luminescent materials exhibiting thermally induced first-order structural phase transitions and can be successfully applied to optimize the thermometric parameters of such thermometers.

CRediT authorship contribution statement

L. Marciniak: Conceptualization, Data curation, Visualization, Formal Analysis, Writing – original draft, Writing – review & editing. **W. Piotrowski:** Data curation, Methodology, Writing – original draft. **M. Szymczak:** Data curation, Methodology, Writing – original draft. **M. Drozd:** Methodology. **V. Kinzhybalo:** Methodology. **M. Back:** Formal analysis, Writing – original draft.

Declaration of competing interest

The authors declare that they have no known competing financial interests or personal relationships that could have appeared to influence the work reported in this paper.

Data availability

Data will be made available on request.

Acknowledgements

This work was supported by the National Science Center (NCN) Poland under project no. DEC-UMO- 2022/45/B/ST5/01629. L.M, W.M.P. would like to acknowledge support from the Polish National Agency For Academic Exchange PPN/BIT/2021/1/00012. M.B would like to acknowledge the support from the Italian Ministry of Foreign Affairs and International Cooperation (MAECI) PPN/BIT/2021/1/00012, PO22MO12. W.M.P. also acknowledges the support from Foundation for Polish Science (FNP) under the START programme.

Appendix A. Supplementary data

Supplementary data to this article can be found online at https://doi.org/10.1016/j.cej.2024.150363.

References

[1] J. Zhou, B. del Rosal, D. Jaque, S. Uchiyama, D. Jin, Nat. Methods 17 (2020) 967.
[2] X. Liu, A. Skripka, Y. Lai, C. Jiang, J. Liu, F. Vetrone, J. Liang, Nat. Commun. 12 (2021) 6401.
[3] R. An, Y. Liang, R. Deng, P. Lei, H. Zhang, Light Sci. Appl. 11 (2022) 217.
[4] E. Ximendes, R. Marin, L.D. Carlos, D. Jaque, Light Sci. Appl. 11 (2022) 237.
[5] S. Yakunin, B.M. Benin, Y. Shynkarenko, O. Nazarenko, M.I. Bodnarchuk, D. N. Dirin, C. Hofer, S. Cattaneo, M.V. Kovalenko, Nat. Mater. 18 (2019) 846.
[6] F. Menges, P. Mensch, H. Schmid, H. Riel, A. Stemmer, B. Gotsmann, Nat. Commun. 7 (2016) 10874.
[7] T. Hartman, R.G. Geitenbeek, G.T. Whiting, B.M. Weckhuysen, Nat. Catal. 2 (2019) 986.
[8] M. Xu, X. Zou, Q. Su, W. Yuan, C. Cao, Q. Wang, X. Zhu, W. Feng, F. Li, Nat. Commun. 9 (2018) 2698.
[9] B. Fond, C. Abram, M. Pougin, F. Beyrau, Opt. Mater. (amst). 89 (2019) 615.
[10] E.C. Ximendes, U. Rocha, B. del Rosal, A. Vaquero, F. Sanz-Rodríguez, L. Monge, F. Ren, F. Vetrone, D. Ma, J. García-Solé, C. Jacinto, D. Jaque, N. Fernández, Adv. Healthc. Mater. 6 (2017) 1601195.
[11] L. Marciniak, K. Kniec, K. Elżbieciak-Piecka, K. Trejgis, J. Stefanska, M. Dramićanin, Coord. Chem. Rev. 469 (2022) 214671.
[12] C. D. S. Brites, A. Millán, L. D. Carlos, In *Handbook on the Physics and Chemistry of Rare Earths* (Eds.: Jean-Claude, B.; Vitalij K., P. B. T.-H. on the P. and C. of R. E.), Elsevier, **2016**, pp. 339–427.
[13] M. Back, J. Ueda, M.G. Brik, T. Lesniewski, M. Grinberg, S. Tanabe, ACS Appl. Mater. Interfaces 10 (2018) 41512.
[14] Y. Zhou, L. Li, F. Qin, Z. Zhang, Opt. Lett. 44 (2019) 4598.
[15] M. Back, J. Ueda, H. Nambu, M. Fujita, A. Yamamoto, H. Yoshida, H. Tanaka, M. G. Brik, S. Tanabe, Adv. Opt. Mater. 9 (2021) 2100033.
[16] C.D.S. Brites, P.P. Lima, N.J.O. Silva, A. Millán, V.S. Amaral, F. Palacio, L.D. Carlos, Nanoscale 4 (2012) 4799.
[17] M. Suta, A. Meijerink, Adv. Theory Simulations 3 (2020) 2000176.
[18] M.D. Dramićanin, J. Appl. Phys. 128 (2020) 40902.
[19] M. Back, J. Ueda, J. Xu, D. Murata, M.G. Brik, S. Tanabe, A.C.S. Appl, Mater. Interfaces 11 (2019) 38937.
[20] L. Marciniak, W. Piotrowski, M. Szalkowski, V. Kinzhybalo, M. Drozd, M. Dramicanin, A. Bednarkiewicz, Chem. Eng. J. 427 (2022) 131941.
[21] S. Wang, J. Zhang, Z. Ye, H. Yu, H. Zhang, Chem. Eng. J. 414 (2021) 128884.
[22] L. Marciniak, W.M. Piotrowski, M. Drozd, V. Kinzhybalo, A. Bednarkiewicz, M. Dramicanin, Adv. Opt. Mater. 10 (2022) 2102856.
[23] M.D. Faucher, O.K. Moune, M.G. Alves, B. Piriou, P. Sciau, M. Pham-Thi, J. Solid State Chem. 121 (1996) 457.
[24] O.K. Moune, J. Dexpert-Ghys, B. Piriou, M.G. Alves, M.D. Faucher, J. Alloys Compd. 275–277 (1998) 258.
[25] M.D. Faucher, P. Sciau, J.M. Kiat, M.G. Alves, F. Bouree, J. Solid State Chem. 137 (1998) 242.
[26] V.A. Antonov, P.A. Arsenev, Z.A. Artykov, D.S. Petrova, J. Appl. Spectrosc. 31 (1979) 1581.
[27] N. Muhammad, A. Khan, S. Haidar Khan, M. Sajjaj Siraj, S.S.A. Shah, G. Murtaza, Phys. B Condens. Matter 521 (2017) 62.
[28] Pechini P. Maggio, Method of preparing iDEAD and alkaline earth titanates and niobates and coating method using the same, Vol. 3,330,697, **1967**, p. US3330697A.
[29] M. Gaft, R. Reisfeld, G. Panczer (Eds.), Modern Luminescence Spectroscopy of Minerals and Materials, Springer, Berlin Heidelberg, Berlin, Heidelberg, 2005, pp. 11–34.
[30] H. Lv, Q. Wu, L. Luo, W. Li, P. Du, J. Phys. Chem. C 127 (2023) 3808.
[31] X. Lai, W. Li, L. Luo, P. Du, J. Alloys Compd. 976 (2024) 173311.
[32] C.D.S. Brites, S. Balabhadra, L.D. Carlos, Adv. Opt. Mater. 7 (2019) 1801239.
[33] J. Xue, T. Hu, F. Li, F. Liu, H.M. Noh, B.R. Lee, B.C. Choi, S.H. Park, J.H. Jeong, P. Du, Laser Photon. Rev. 17 (2023) 2200832.
[34] M. Back, E. Trave, J. Ueda, S. Tanabe, Chem. Mater. 28 (2016) 8347.